Simultaneous measurement of β-delayed proton and γ decay of ^{27}P

E. McCleskey,[1,*] A. Banu,[1,†] M. McCleskey,[1] T. Davinson,[2] D. T. Doherty,[2,‡] G. Lotay,[2,§] B. T. Roeder,[1] A. Saastamoinen,[3,¶] A. Spiridon,[1] L. Trache,[1,**] J. P. Wallace,[2] P. J. Woods,[2] and R. E. Tribble[1]

[1]*Cyclotron Institute, Texas A & M University, College Station, Texas 77843-3366, USA*

[2]*School of Physics and Astronomy, University of Edinburgh, Edinburgh EH9 3JZ, United Kingdom*

[3]*Department of Physics, University of Jyväskylä, P.O. Box 35 (YFL), FI-40014, Finland*

(Received 20 August 2015; revised manuscript received 24 July 2016; published 27 December 2016)

This is the first study of ^{27}P to measure both the β-delayed proton and β-delayed γ decays. While no new proton groups in the astrophysically interesting energy region of 300–400 keV were observed, a new upper limit on the proton branching of 0.16% was estimated. Several new γ-ray lines were observed, mainly coming from the isobaric analog state in ^{27}Si, which has been assigned a more accurate energy value of 6638(1) keV.

DOI: 10.1103/PhysRevC.94.065806

I. INTRODUCTION

^{26}Al has an interesting level structure, in that it has a long-lived ($t_{1/2} = 6.34$ s) state only 228 keV above its ground state [1]. The β decay of the ground state of ^{26}Al populates an excitation state in ^{26}Mg* which then emits a characteristic γ ray with an energy of 1.809 MeV. Because the half-life of the ground state of ^{26}Al ($t_{1/2} = 7.2 \times 10^5$ yr) is shorter than the age of our solar system, the observation of this γ-ray line [2] provides evidence of on-going nucleosynthesis. Further proof comes from astrophysical observations made by the COMPTEL sky map [3], which demonstrated that ^{26}Al is far more prominent along the galactic plane and at the galactic center, regions known to contain very massive hot young stars. However, the main sites for the creation and destruction of ^{26}Al are currently under debate, although recent studies point to Wolf-Rayet (WR) stars as being the main source of ^{26}Al [4,5].

Due to the large spin difference between the ground state (^{26}Al$^g = 5^+$) and the isomeric state (^{26}Al$^m = 0^+$), transitions between the two levels are highly suppressed in stellar environments where temperatures are below about $T = 0.4$ GK. However, in environments above $T = 0.4$ GK, such as oxygen-neon (ONe) novae and core collapse supernovae (CCSN), they can be linked via thermal excitation to higher lying levels in ^{26}Al [5]. As a result of this, it is possible that a slow drain of the ^{26}Al nuclei from the metastable state to the ground state is occurring as the temperature is increased [6]. Therefore, understanding reactions involving both the ground state and the isomeric state is essential in identifying all of the astrophysical locations for production and destruction of ^{26}Al.

The dominant destruction method for both ^{26}Al^g and ^{26}Al^m is radiative proton capture. In the low-energy region of interest, the reaction rates are dominated by narrow, isolated resonances [5]. At different temperatures (and therefore energies), different resonances will dominate the destruction reactions. The properties for each resonance (energy, spin, and parity) as well as their partial γ and proton widths must be determined to understand their contribution to the astrophysical radiative proton capture reaction rate. This study focused on resonances relevant to the isomeric state in ^{26}Al.

A resonance at 146.3(3) keV, corresponding to the $5/2^+$ 7837.6(2)-keV level in ^{27}Si, is important in the temperature region of $T = 0.02$–0.20 GK and therefore important in WR and asymptotic giant branch (AGB) stars as well as in classical novae (CN). In the temperature region that covers both ONe novae and CCSN, $T = 0.10$–1.00 GK, a resonant energy of 378.3(30) keV corresponding to the $3/2^-$ 8069.6(30)-keV level in ^{27}Si dominates the reaction rate. For temperatures above $T = 1.00$ GK, relating mainly to the CCSN environment, several resonant energies contribute to the reaction rate, namely, those at 378.3(30), 447.7(6), 631.7(25), and 684.2(9) keV. These relevant resonances are listed in Table I [7].

An experiment done at Argonne National Laboratory (ANL) using the ATLAS accelerator and the Gammasphere array [8] to investigate ^{27}Si provided information on important resonant energies for both ^{26}Al$^g(p,\gamma)^{27}$Si and ^{26}Al$^m(p,\gamma)^{27}$Si [9,10]. New levels in ^{27}Si were identified, energy values for previously observed levels were obtained with greater precision, and spin and parity values for most levels were assigned. Two resonant energies not observed in [9,10] due to spin and parity selection rules are 485 and 632 keV, relating to the 8176(3)- and 8318(3)-keV levels in ^{27}Si respectively. Both are tentatively assigned a $(1/2 \text{ or } 3/2)^+$ value [7].

The ANL ^{27}Si experiment mentioned above favored the population of high-spin states above the proton threshold (S_p) in ^{27}Si, which were ideal for investigating proton decays to the 5^+ ground state in ^{26}Al. The study presented in this paper focused on proton decays to the 0^+ isomeric state which required the population of low-spin states in ^{27}Si above the proton threshold of that level [$E^* > S_p + E(0^+) = 7.463 + 0.228 = 7.691$ MeV]. As such, a different approach

*emccleskey@comp.tamu.edu

†Present address: Department of Physics and Astronomy, James Madison University, Harrisonburg, VA 22807.

‡Present address: CEA Saclay, Gif-sur-Yvette 91400, France.

§Present address: University of Surrey, Guildford, Surrey, GU2 7XH, United Kingdom.

¶Present address: Texas A and M Cyclotron Institute, College Station, Texas 77843.

**Present address: National Institute for Physics and Nuclear Engineering, Bucharest-Magurele, Romania.

TABLE I. Relevant resonances for $^{26}\mathrm{Al}^{m}(\mathrm{p},\gamma)^{27}\mathrm{Si}$ [9,10].

E_{res} (keV)	E_x (keV)	Temp. range (GK)	Site
146.3(3)	7837.6(2)	0.02–0.20	WR, AGB, CN
378.3(30)	8069.6(30)	0.10–1.00	ONe, CCSN
447.7(6)	8139.0(6)	>1.00	CCSN
631.7(25)	8328(2)	>1.00	CCSN
684.2(9)	8375.5(9)	>1.00	CCSN

than the one successfully used for the ANL experiment was required to gain information on the isomeric proton capture reaction [$^{26}\mathrm{Al}^{m}(p,\gamma)^{27}\mathrm{Si}$] of interest. However, this (p,γ) reaction is very difficult to measure directly due to the fact that the proton must tunnel through the Coulomb barrier, giving it a very small cross section. Thus, an indirect method was utilized, that of the β-delayed proton and γ decay of ^{27}P.

This indirect approach involves ^{27}P first decaying to ^{27}Si, the same compound system as the direct approach, which is why we can compare the indirect method to the direct method. States populated above the proton threshold in ^{27}Si can decay by proton emission to $^{26}\mathrm{Al}^{m}$. These are the states of interest since they represent the resonance states in the time-reversed proton capture reaction. The selection rules governing the β decay are favorable to the population of spin $1/2^{+}$ and spin $3/2^{+}$ levels in ^{27}Si, which increases the probability of identifying the 485- and 632-keV resonances mentioned previously, if they do indeed exist. This experiment was the first to look at γ decays from excited states in ^{27}Si that were populated from the β decay of ^{27}P.

Prior observations of the β-delayed proton decay of ^{27}P [11,12] were made at the Lawrence Berkeley National Laboratory (LBNL). In these experiments, proton beams from the LBNL 88-in. cyclotron of 28 and 45 MeV were used to bombard targets made of natural silicon. The reaction products were thermalized in helium gas and then transported to a rotating catcher wheel directly in front of silicon detectors. Four proton groups were identified with energies of 466(3), 612(2), 731(2), and 1324(4) keV in the laboratory frame. An overall β-delayed proton branch of 0.07% was obtained by Ognibene *et al.* [12] by comparing their result to the known ^{28}P β-delayed proton branch. This was done by using the relative proton yields of ^{27}P and ^{28}P as well as their production cross sections, which were calculated using the statistical-model fusion-evaporation code ALICE [13]. However, due to the unavoidable presence of ^{24}Al, a weak $\beta\alpha$ emitter, there was a background in the form of a continuum between 300 and 1100 keV in their proton spectrum. Thus, it was not possible to obtain a total β-decay strength because low-energy protons could not be unambiguously assigned. It was in search of these low-energy protons that the present study was undertaken.

II. EXPERIMENTAL SETUP

This experiment was done at the Texas A&M University (TAMU) Cyclotron Institute using the K500 superconducting cyclotron and the Momentum Achromat Recoil Spectrometer (MARS) [14]. A primary beam of ^{28}Si at 40 MeV/u was

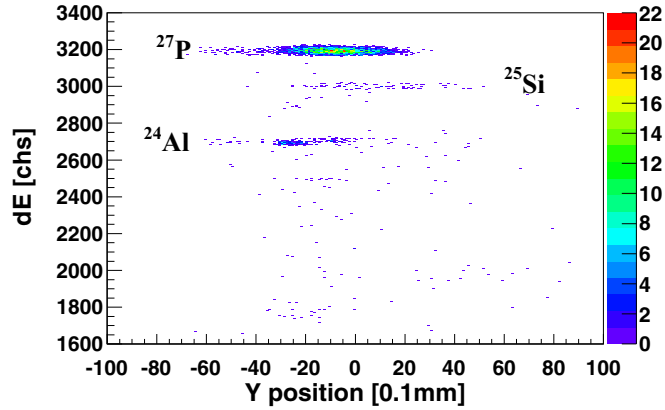

FIG. 1. Final beam composition and identification with the ΔE silicon detector from the telescope located at the end of MARS with the momentum spread of the beam at $\Delta p/p = \pm 0.25\%$. The vertical axis represents the energy deposited (arbitrary units) and the horizontal axis represents the position in the focal plane of MARS.

impinged upon a liquid-nitrogen-cooled H_2 target kept at a pressure of 2 atm. The fragment of interest, ^{27}P, was separated with a purity of 82% and an energy of approximately 35 MeV/u at the end of MARS, where a ΔE-E silicon telescope (1 mm and 500 μm thick, respectively) was placed in the focal plane. The momentum spread of the beam was controlled by mechanical slits located upstream of the experimental setup after dipole 1 in MARS. Figure 1 shows the beam resulting from the final configuration with the momentum-defining slits set such that the momentum spread of the beam was $\Delta p/p = \pm 0.25\%$, as required for proper implantation, discussed below. This configuration resulted in a production rate of 10 particles per second for ^{27}P. The important impurities, with regards to the experiment, consisted mainly of ^{25}Si (2%) and ^{24}Al (8%), but also small amounts (less than 1%) of ^{28}P, ^{27}Si, ^{26}Si, and ^{22}Mg.

The implantation-decay station, located at the very end of MARS, was redesigned for this experiment to greatly improve the γ-ray efficiency without compromising the proton efficiency or resolution achieved by the original design [15]. The setup included a sandwich of three silicon detectors from Micron Semiconductor Ltd. [16] kept at a 45° angle to the beam to allow a high-purity germanium detector (HPGe) to be placed on either side of the point of implantation. The top view of the implantation and decay station is shown in Fig. 2. The center silicon detector was a Mircon BB2 double-sided silicon strip detector (DSSSD), referred to as the proton detector because this was where the ^{27}P was implanted and the protons of interest were studied. The front and back silicon detectors, referred to as the $\beta 1$ and $\beta 2$ detectors, respectively, aided in the implantation process, discussed below, and were used to detect β particles during the decay measurement. All three of these silicon detectors were cooled with cold flowing water (20 °C) in order to reduce the leakage currents and therefore improve energy resolution.

Implantation was achieved using a rotating 11 mil (279.4 μm) aluminum degrader placed in front of the silicon sandwich. Changing the angle of this degrader changed the

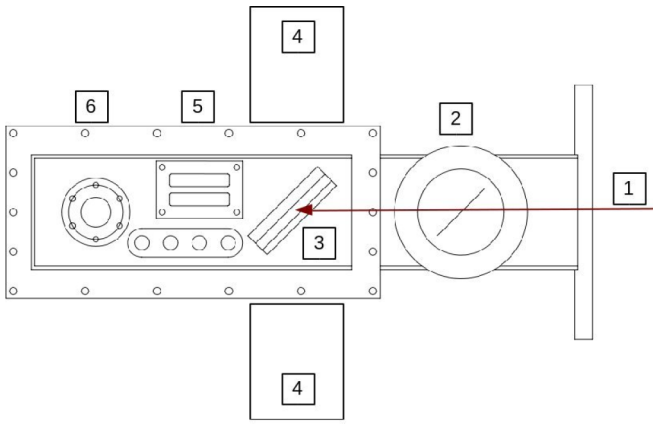

FIG. 2. Top view of the implantation-decay station placed at the end of MARS where [1] beam, [2] rotating aluminum degrader, [3] silicon detectors (the order in which the beam sees them is $\beta 1$, proton detector, and then $\beta 2$), [4] HPGe detectors, [5] electronic feed-through, and [6] water cooling system input.

energy deposited, and therefore the implantation depth of the beam products. Monitoring the energy deposited in the $\beta 1$ and the proton detectors made it possible to find the correct angle needed to implant ^{27}P only in the proton detector, shown in Fig. 3. The elements along the approximate 45° diagonal represent nuclei that punch through both the $\beta 1$ and the proton detector. In this case, these nuclei are the beam impurities mentioned earlier, and with the exception of ^{25}Si and ^{24}Al, make up only a small fraction of the beam. As they completely pass through the proton detector, they do not interfere with the proton measurement. The bend at the upper right corner of the plot represents when beam products begin to stop in the proton detector. After this corner is turned, nuclei are fully stopped and deposit most of their energy in the proton detector. Implantation was also aided by restricting the momentum

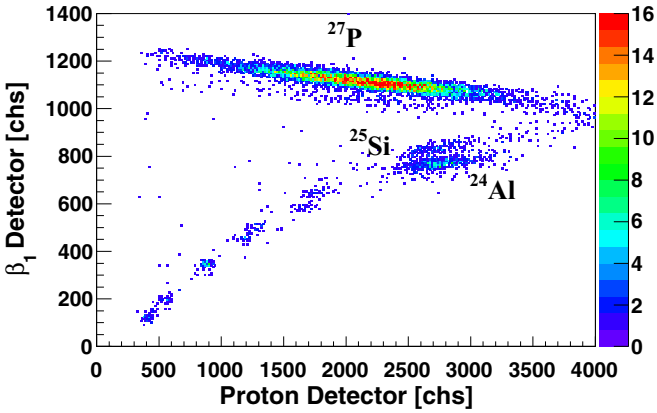

FIG. 3. Implantation of ^{27}P in the proton detector. The y axis shows the energy deposited in the $\beta 1$ detector and the x axis shows the energy deposited in the proton detector. Nuclei along the approximate 45° diagonal punch through both detectors and therefore do not interfere with the proton measurement. Only after the corner in the upper right of the figure is passed are the nuclei stopped in the proton detector.

spread of the beam using the momentum-defining slits in MARS. This ensured that the ^{27}P and the low-energy protons of interest were fully contained within the proton detector.

The technique used in this experiment was similar to experiments done previously at TAMU [17–20]. The beam from the cyclotron was pulsed by sending electronic signals (beam-on and beam-off requests) to the cyclotron, with the ^{27}P implanted for 503 ms into the proton detector; the cyclotron was then turned off for a 3-ms wait (to give the cyclotron time to process the beam-off request), then the decay was measured for 500 ms, roughly twice the half-life value 260(80) ms [11]. This allowed the β-p and the β-γ coincidences to be measured simultaneously. All decay data were taken with the condition of a logical OR between protons and β-γ coincidences. That is, when an event occurred in the proton detector or there was a β-γ coincidence (an event in either β detector and a simultaneous event in either HPGe detector), data were recorded.

Two different configurations for the proton silicon detector were used in this experiment. The first used the thinner DSSSD (50 μm thick, 24 strips front and back, 1 mm in width) as the proton detector. The thinner proton detector was ideal in looking for low-energy protons from the decay of ^{27}P due to its small pixel volume which helped reduce the β contribution, discussed in the next section. This proton detector was later replaced with a thicker DSSSD (104 μm, 24 strips front and back, 1 mm in width) in order to study the γ rays from the decay of the ^{27}Si levels populated from the β decay of ^{27}P. The thicker detector permitted the momentum slits to be opened farther, allowing more beam to be implanted. In both configurations the $\beta 1$ detector was a 300 μm thick silicon strip detector and the $\beta 2$ detector was 1 mm thick, 5×5 cm^2 silicon-pad detector. Regardless of which proton detector was in place, two HPGe detectors were used, one of which was placed in a lead barrel-shaped housing to be fully shielded while the other HPGe detector had improvised shielding in the form of cadmium and copper sheets wrapped around the detector capsule.

III. RESULTS

A. Proton study

The proton spectra were obtained by first gain matching all strips on the front and all strips on the back using α sources. Then, steps were taken to reduce the background, which mostly came from β particles, higher energy protons, and α particles that deposited only some of their energy in the detector. The first step involved a restriction on the multiplicity. Events in which multiple pixels recorded data were rejected, leaving only cases where the multiplicity was unity ($m = 1$). Cases where the multiplicity was higher than unity were either coincident noise, β particles traveling along the detector through several strips, or the rare event where the ^{27}Si was implanted very near the gap between strips, allowing the emitted protons to travel through two strips.

The second step was create a requirement that the energy deposited in the horizontal strips (E_x) be approximately equal to the energy deposited in the vertical strips (E_y). This was

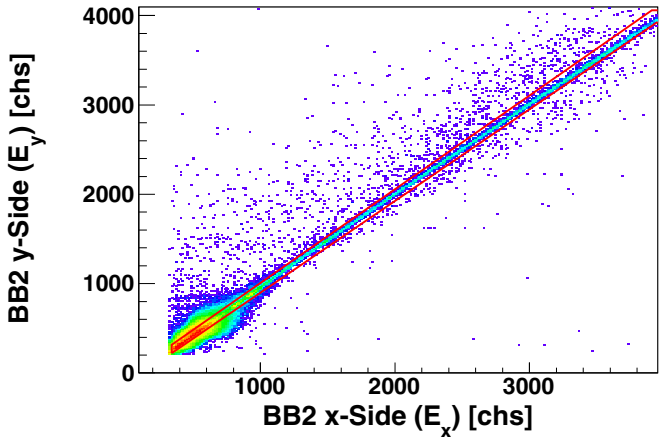

FIG. 4. Gate created for the $E_x = E_y$ condition is shown in red for the thicker proton detector with the $m = 1$ condition applied.

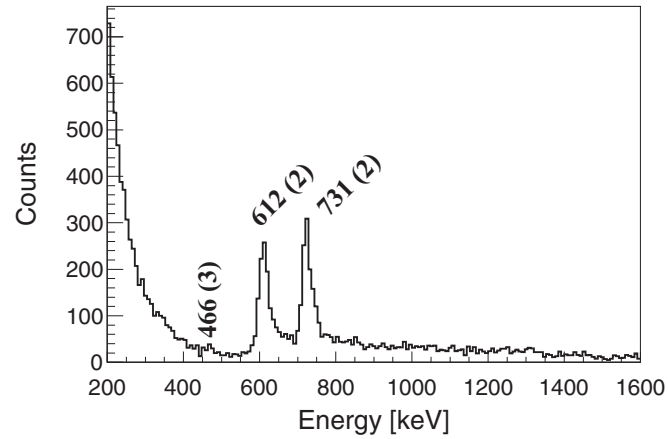

FIG. 5. Proton spectrum obtained from the thinner proton detector with the $m = 1$ and $E_x = E_y$ conditions applied. Energy values from Ref. [12].

achieved by the placement of a tight gate around the diagonal line in the two-dimensional histogram shown in Fig. 4. This gate removed much of the background that made it past the $m = 1$ condition. However, even with these cuts, background in the proton spectra remained a problem, which was why a proton branch value could not be accurately determined in this measurement. Only an upper limit could be estimated with these data.

An internal energy calibration was done by implanting ^{28}P in the center of the proton detector and measuring its β-delayed protons which are in the energy region of interest. However, ^{28}P has a much lower proton branch than ^{27}P (1.3×10^{-3} % versus the predicted 0.07% for ^{27}P). This was somewhat mitigated by the fact that ^{28}P was created about 5 times more abundantly than ^{27}P in this experiment. What was measured in the detector was not the true proton energy in the laboratory system, but because of the implantation process, a combination of the proton energy, the recoil energy of the daughter heavy ion (after the proton decay), and the small amount of energy deposited in the detector from the β particles [15,17]. Limited statistics resulted in only the ability to confirm the proton energies from the previous measurement [12]. The final proton results are shown in Fig. 5 with the $m = 1$ and $E_x = E_y$ conditions applied. The β background is clearly the dominate feature in the low-energy region, negatively effecting the signal-to-noise ratio of the 466-keV proton. As a result of these low statistics, no new protons could be identified.

The calculation of the absolute proton branch (B_{abs}) was done using the number of observed protons (N_p), normalized to the number of 780.8-keV γ rays (N_γ) observed with efficiency ϵ_{abs}

$$B_{\text{abs}} = \frac{N_p}{N_\gamma/[\epsilon_{abs}(E_\gamma)I_\gamma(E_\gamma)]}.$$

This γ-ray line from the energy spectrum shown in Fig. 6, was chosen due to its intensity and because it was in the energy range of the calibration sources and thus its efficiency could be accurately determined. The absolute intensity (I_γ) of this γ ray was found to be 40.66(24)%. An upper limit of 0.16% on the absolute proton branch for ^{27}P was estimated in this study. This is much lower than anything previously measured with this experimental setup, as ^{23}Al had a 1.22% and ^{31}Cl had a 0.70% proton branch, respectively [11,17]. The lower the proton branch, the more likely it is that β particles dominate the spectrum, negatively affecting the proton signal-to-noise ratio.

B. γ study

The γ-ray spectra were obtained using two HPGe detectors placed on either side of the implantation-decay station and centered on the point of implantation in the proton detector. The γ-ray energy and efficiency calibrations were done using sources (^{60}Co, ^{137}Cs, and ^{152}Eu) up to energies around 1.8 MeV and then extended up to 8 MeV using well-known β-delayed γ rays from ^{24}Al [21,22], which was implanted into the thicker proton detector at the same location as the ^{27}P was implanted. The only background present in all γ-ray spectra were beam related. Specifically, known β-delayed γ rays from ^{22}Mg, ^{26}Si, and ^{28}P were identified in the spectra and used in the extended calibrations. This background arose because of timing correlations with our subject of interest. Further background reduction was then achieved using time gating.

Previously observed γ rays from ^{27}Si [9,10] were identified in the β-delayed spectrum as well as several newly observed γ rays, which are shown in Fig. 6. A summary of all ^{27}Si γ rays is shown in Table II. Most new γ rays identified in this study came from the isobaric analog state (IAS) but a few γ rays were observed coming from other known levels.

From the $1/2^+$ IAS, the most intense γ rays resulted from transitions to the $3/2^+$ 957.1-keV level and to the $1/2^+$ 780.8-keV level. Other, less intense γ rays, came from transitions to the $1/2^+$ 3539.8-keV level and to the $5/2^+$ ground state. It is also suggested here that a 3775(1)-keV γ ray arises from a transition to the $3/2^+$ 2866.0-keV state. While this last γ-ray line corresponds energetically to a double escape peak from the 4792.3-keV γ ray, this peak was far more intense than what was expected for an escape peak. These γ rays established an IAS level energy of 6638(1) keV [vs the 6626(3) keV predicted [23,24]]. The large difference in IAS energies

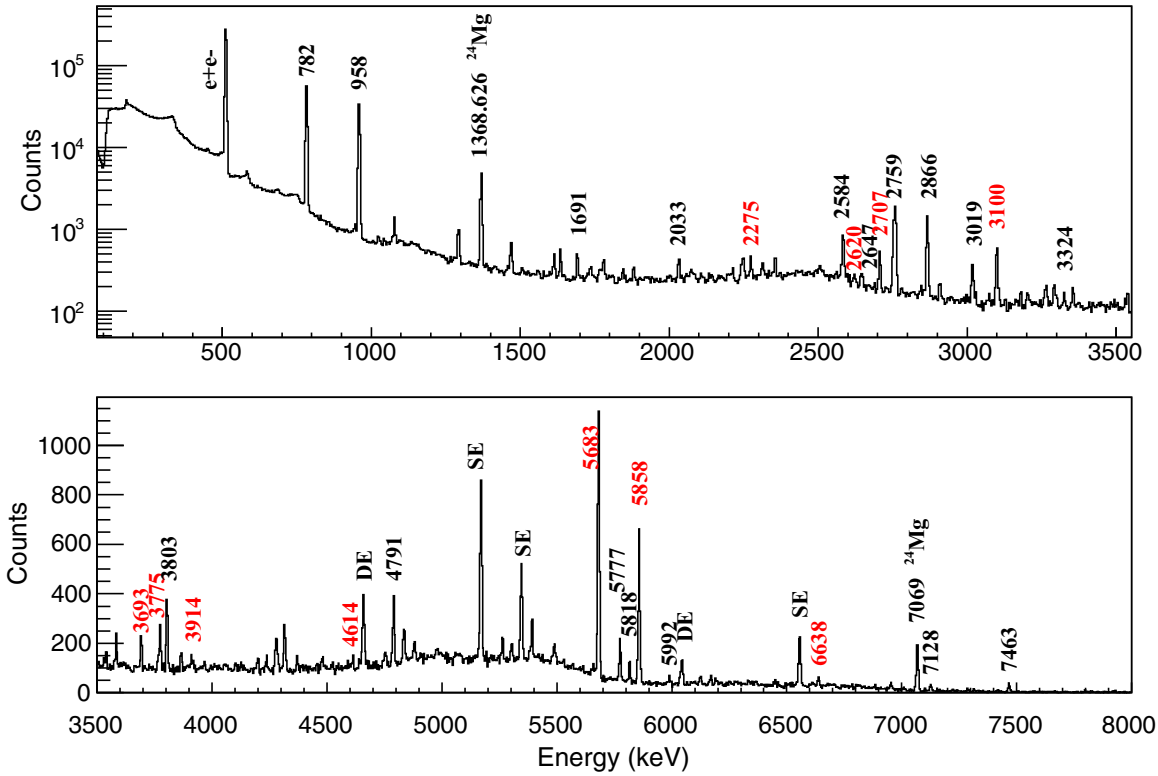

FIG. 6. The ^{27}Si γ-ray spectrum created from the total statistics obtained from HPGe 2. The top portion covers 0–3.5 MeV and the bottom section covers 3.5–8 MeV. All new ^{27}Si γ rays are shown in red. All large peaks not coming directly from ^{27}Si have also been labeled. They consist of single escapes (SE), double escapes (DE), and impurities (β-delayed γ decay of ^{24}Al).

might be due to the high density of levels and the constant α contamination observed in the previous reaction study using ^{28}Si(^{3}He ,α)^{27}Si [24].

Several new γ transitions were observed coming from the $3/2^+$ 6559.0-keV level, one from the transition to the $3/2^+$ 2866.0-keV level and two less intense γ rays from transitions to the $5/2^+$ levels (4284.8 keV and 2647.2 keV). The observation of these two $5/2^+$ feed-in γ rays explained why known γ-ray lines were observed coming from the deexcitation of levels not directly populated by the β decay in this experiment. A couple of less intense γ rays coming from a transition of the $3/2^+$ 7325.4-keV level and from the $1/2^+$ 5573.7-keV level were also observed.

The previously observed γ-ray line arising from the transition from the 7468.8-keV level $(1/2, 5/2)^+$ to the ground state was observed here without any higher lying γ rays populating the initial 7468.8-keV level suggests that this level is indeed $1/2^+$ and is populated by the original β decay. Lastly, the newly identified 2707(1)-keV γ-ray line is possibly the result of more than one transition. Two possibilities include γ rays emitted from the $1/2^+$ 5573.7-keV level and from the $3/2^+$ 6513-keV level. Due to the lack of statistics, further clarification regarding this γ-ray line could not be made in this study.

The β branch and log ft values were calculated by first assuming the pandemonium effect [25,26] was small enough that our uncertainty values fully accounted for these cases. The pandemonium effect occurs when weak γ transitions, mainly from highly excited levels populated by the original β decay, are unlikely to be observed due to the detector efficiency in this energy region. If this effect is larger than expected, it would mean that the level populations discussed below are over estimated. Second, the spin difference between ^{27}P and the ground state of ^{27}Si signifies that β decays to the ground state are highly suppressed and therefore would not significantly contribute to the observed β branch.

The level populations (I^i_{level}) were found by subtracting the total number of γ rays populating that level ($N_{\gamma_{\text{in}}}$) from the total number of γ rays emitted from that level ($N_{\gamma_{\text{out}}}$)

$$I^i_{\text{level}} = \left(\sum N^i_{\gamma_{\text{out}}}\right) - \left(\sum N^i_{\gamma_{\text{in}}}\right),$$

and then the β-branch values for each level were calculated using

$$B^i_{\text{level}}(\%) = \frac{I^i_{\text{level}}}{\sum I^i_{\text{level}}} \times 100.$$

The log ft values were calculated using the half-life value of ^{27}P [260(80) ms], the ground-state to ground-state Q value [11.669(26) MeV] and the LOGFT analysis program provided by the NNDC website [27]. The log ft value of 3.30(14) for the 6638-keV level verified that it was indeed the IAS. The β branch and log ft values for each level can be seen in Table III. A new partial-decay scheme for ^{27}P was created using the results of this study, combined with relevant information from Refs. [9,10], and can be seen in Fig. 7. The γ-ray lines were

TABLE II. ^{27}P β-delayed γ observed in this experiment. All level energies are from [10] except that of the IAS at 6638, first observed here and denoted by $*$.

E_γ (keV)	I_γ (%)	E_i (keV)	J_i^π	E_f (keV)	J_f^π
782(1)	100	780.8(1)	$\frac{1}{2}^+$	0.0	$\frac{5}{2}^+$
958(1)	73.11(47)	957.1(1)	$\frac{3}{2}^+$	0.0	$\frac{5}{2}^+$
1691(1)	0.79(9)	2647.2(1)	$\frac{5}{2}^+$	957.1(1)	$\frac{3}{2}^+$
2033(1)	0.87(11)	5573.7(3)	$\frac{1}{2}^+$	3539.8(1)	$\frac{1}{2}^+$
2275(1)	0.93(13)	6559.0(2)	$\frac{3}{2}^+$	4284.8(2)	$\frac{5}{2}^+$
2584(1)	3.74(18)	3539.8(1)	$\frac{1}{2}^+$	957.1(1)	$\frac{3}{2}^+$
2620(2)	0.17(7)	7325.4(18)	$\frac{3}{2}^+$	4705.1(2)	$\frac{5}{2}^+$
2647(2)	0.29(7)	2647.2(1)	$\frac{5}{2}^+$	0.0	$\frac{5}{2}^+$
2707(1)	1.51(12)	5573.7(3)	$\frac{1}{2}^+$	2866.0(3)	$\frac{3}{2}^+$
		6513(4)	$\frac{3}{2}^+$	3803.1(2)	$\frac{3}{2}^+$
2759(1)	11.70(25)	3539.8(1)	$\frac{1}{2}^+$	780.8(1)	$\frac{1}{2}^+$
2866(1)	6.34(18)	2866.0(3)	$\frac{3}{2}^+$	0.0	$\frac{5}{2}^+$
3019(1)	0.91(12)	6559.0(2)	$\frac{3}{2}^+$	3539.8(1)	$\frac{1}{2}^+$
		3803.1(2)	$\frac{3}{2}^+$	780.8(1)	$\frac{1}{2}^+$
3100(1)	3.04(15)	6638(1)*	$\frac{1}{2}^+$	3539.8(1)	$\frac{1}{2}^+$
3324(2)	0.67(15)	4284.8(2)	$\frac{5}{2}^+$	957.1(1)	$\frac{3}{2}^+$
3693(1)	0.86(13)	6559.0(2)	$\frac{3}{2}^+$	2866.0(3)	$\frac{3}{2}^+$
3775(1)	1.78(19)	6638(1)*	$\frac{1}{2}^+$	2866.0(3)	$\frac{3}{2}^+$
3803(1)	2.07(15)	3803.1(2)	$\frac{3}{2}^+$	0.0	$\frac{5}{2}^+$
3914(1)	0.40(13)	6559.0(2)	$\frac{3}{2}^+$	2647.2(1)	$\frac{5}{2}^+$
4614(1)	0.38(9)	5573.7(3)	$\frac{1}{2}^+$	957.1(1)	$\frac{3}{2}^+$
4791(1)	3.33(24)	5573.7(3)	$\frac{1}{2}^+$	780.8(1)	$\frac{1}{2}^+$
5683(1)	15.78(39)	6638(1)*	$\frac{1}{2}^+$	957.1(1)	$\frac{3}{2}^+$
5777(1)	2.55(20)	6559.0(2)	$\frac{3}{2}^+$	780.8(1)	$\frac{1}{2}^+$
5818(1)	1.18(15)	6776.3(8)	$\frac{1}{2}^+$	957.1(1)	$\frac{3}{2}^+$
5858(1)	9.00(30)	6638(1)*	$\frac{1}{2}^+$	780.8(1)	$\frac{1}{2}^+$
5992(1)	0.20(8)	6776.3(8)	$\frac{1}{2}^+$	780.8(1)	$\frac{1}{2}^+$
6638(1)	1.11(16)	6638(1)*	$\frac{1}{2}^+$	0.0	$\frac{5}{2}^+$
7128(1)	0.61(11)	7909.1(7)	$\frac{3}{2}^+$	780.8(1)	$\frac{1}{2}^+$
7463(3)	0.99(14)	7468.8(8)	$\frac{1}{2}^+$	0.0	$\frac{5}{2}^+$

placed in the partial-decay scheme based on γ-decay spin and parity selection rules as well as their energy values.

IV. DISCUSSION

This study of the β-delayed proton and γ decay of ^{27}P was undertaken in the hopes of finding new proton groups of astrophysical relevance. Despite the use of an improved implantation-decay station design that allowed the HPGe detectors to be moved in as close to the point of implantation as physically possible, the proton branch was so low compared to the background that new transitions could not be observed. An upper limit to the proton branch was estimated at 0.16%, higher than the previous measurement [12], probably due to

TABLE III. Measured ^{27}P β-branching and log ft values. All energies are from [10] except the IAS at 6638, denoted by $*$.

E_{level} (keV)	Our J^π	Ref. [10]	B^i_{level}	log ft
780.8 (1)	$\frac{1}{2}^+$	$\frac{1}{2}^+$	38.80(45)	4.76(14)
957.1 (1)	$\frac{3}{2}^+$	$\frac{3}{2}^+$	27.45(38)	4.87(14)
2866.0 (3)	$\frac{3}{2}^+$	$\frac{3}{2}^+$	2.00(16)	5.55(14)
3539.8 (1)	$\frac{1}{2}^+$	$\frac{1}{2}^+$	5.74(21)	4.91(14)
3803.1 (2)	$\frac{3}{2}^+$	$\frac{3}{2}^+$	0.79(12)	5.70(15)
5573.7 (3)	$\frac{1}{2}^+$	$\frac{1}{2}^+$	3.30(17)	4.47(14)
6513 (4)	$\frac{3}{2}^+$	$\frac{3}{2}^+$	0.82(7)	4.66(14)
6559.0 (2)	$\frac{3}{2}^+$	$\frac{3}{2}^+$	2.57(18)	4.14(14)
6638 (1)*	$\frac{1}{2}^+$	$\frac{1}{2}^+$	16.63(33)	3.30(14)
6776.3 (8)	$\frac{1}{2}^+$	$\frac{1}{2}^+$	0.75(9)	4.57(15)
7468.8 (8)	$\frac{1}{2}^+$	$(\frac{1}{2},\frac{5}{2})^+$	0.54(8)	4.33(15)
7909.1 (7)	$\frac{3}{2}^+$	$\frac{3}{2}^+$	0.62(9)	3.98(15)

the fact that the experiment discussed here observed both the protons and the γ rays, and therefore, allowed a true coincidence measurement to be taken. In contrast, the previous measurement depended upon comparing to the relative proton yield of ^{28}P and used reaction modeling to obtain cross sections. Since the IAS is below the proton separation energy, characterizing this as a weak β-delayed proton emitter, the β background was the dominate feature in the low-energy region of the silicon detectors, despite major improvements to our experimental setup. Further investigations in this region should continue along the lines of a gas-filled detector [28].

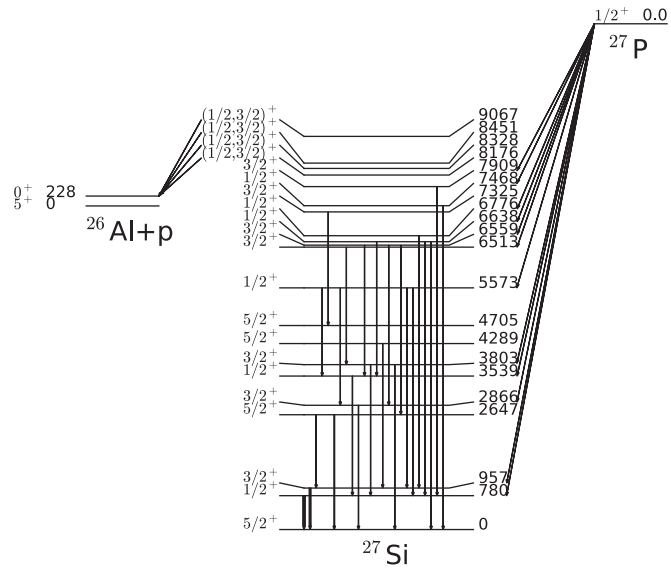

FIG. 7. Partial-decay scheme for ^{27}P with the most intense β decays shown. Line thickness corresponds directly with intensity. Thus, the most intense transitions are represented by the thickest arrows.

The experimental setup used in this study, however, yielded a higher γ-ray efficiency than in previous β-delayed proton decay experiments. This, coupled with few γ-emitting impurities, allowed the observation of several new γ-ray lines, mostly γ rays emitted from the IAS, which itself had a new and more accurate energy value assigned [6638(1)], as this was the first measurement where the IAS was populated directly by β decay. Also, the 7463(3)-keV level appears to have a spin of $1/2^+$, but more data are needed before a positive identification can be made.

ACKNOWLEDGMENTS

This work was supported by the DOE Office of Nuclear Physics Grant No. DE-FG02-93ER40773, and NNSA SSAA Grants No. DE-NA0001785 and No. DE-NA0001786.

[1] J. M. Freeman, J. G. Jenkin, G. Murray, D. C. Robinson, and W. E. Burcham, Nucl. Phys. A **132**, 593 (1969).
[2] W. A. Mahoney, J. C. Ling, A. S. Jacobson, and R. E. Lingenfelter, Astrophys. J. **262**, 742 (1982).
[3] R. Diehl, C. Dupraz, K. Bennett, H. Bloemen, W. Hermsen, J. Knoedlseder, G. Lichti, D. Morris, J. Ryan, V. Schoenfelder, H. Steinle, A. Strong, B. Swanenburg, M. Varendorff, and C. Winkler, Astron. Astrophys. **298**, 445 (1995).
[4] B. Carroll and D. Ostlie, *An Introduction to Modern Astrophysics* (Addison-Wesley, Reading, MA, 1996).
[5] C. Iliadis, *Nuclear Physics of Stars* (Wiley-VCH, New York, 2007).
[6] R. C. Runkle, A. E. Champagne, and J. Engel, Astrophys. J. **556**, 970 (2001).
[7] G. Lotay, P. J. Woods, D. Seweryniak, M. P. Carpenter, R. V. F. Janssens, and S. Zhu, Phys. Rev. C **80**, 055802 (2009).
[8] I. Y. Lee, Nucl. Phys. A **520**, c641 (1990).
[9] G. Lotay, P. J. Woods, D. Seweryniak, M. P. Carpenter, R. V. F. Janssens, and S. Zhu, Phys. Rev. Lett. **102**, 162502 (2009).
[10] G. Lotay, P. J. Woods, D. Seweryniak, M. P. Carpenter, H. M. David, R. V. F. Janssens, and S. Zhu, Phys. Rev. C **84**, 035802 (2011).
[11] J. Aysto, X. J. Xu, D. M. Moltz, J. E. Reiff, J. Cerny, and B. H. Wildenthal, Phys. Rev. C **32**, 1700 (1985).
[12] T. J. Ognibene, J. Powell, D. M. Moltz, M. W. Rowe, and J. Cerny, Phys. Rev. C **54**, 1098 (1996).
[13] M. Blann, Lawrence Livermore National Laboratory Report, 1983 (unpublished).
[14] R. E. Tribble, R. H. Burch, and C. A. Gagliardi, Nucl. Instrum. Methods Phys. Res. Sect. A **285**, 441 (1989).
[15] M. McCleskey, L. Trache, A. Saastamoinen, A. Banu, E. Simmons, B. T. Roeder, G. Tabacaru, R. E. Tribble, T. Davinson, P. J. Woods, and J. Aysto, Nucl. Instrum. Methods Phys. Res. Sect. A **700**, 124 (2013).
[16] Micron Semiconductor Ltd., Lancing, Sussex, England.
[17] A. Saastamoinen, L. Trache, A. Banu, M. A. Bentley, T. Davinson, J. C. Hardy, V. E. Iacob, M. McCleskey, B. T. Roeder, E. Simmons, G. Tabacaru, R. E. Tribble, P. J. Woods, and J. Aysto, Phys. Rev. C **83**, 045808 (2011).
[18] L. Trache, A. Banu, J. C. Hardy, V. E. Iacob, M. McCleskey, E. Simmons, G. Tabacaru, R. E. Tribble, J. Aysto, A. Jokinen, A. Saastamoinen, M. A. Bentley, D. Jenkins, T. Davinson, P. J. Woods, N. L. Achouri, and B. T. Roeder, in Proceedings of Tenth Symposium on Nuclei in the Cosmos, PoS (NIC-X) 163 (2008).
[19] L. Trache, Fourth International Conference on Proton-emitting Nuclei (PROCON2011), June 2011, Bordeaux, France.
[20] J. P. Wallace, P. J. Woods, G. Lotay, A. Alharbi, A. Banu, H. M. David, T. Davinson, M. McCleskey, B. T. Roeder, E. Simmons, A. Spiridon, L. Trache, and R. E. Tribble, Phys. Lett. B **712**, 59 (2012).
[21] J. Honkanen, M. Kortelahti, J. Aysto, K. Eskola, and A. Hautojarvi, Phys. Scr. **19**, 239 (1979).
[22] E. K. Warburton, C. J. Lister, D. E. Alburger, and J. W. Olness, Phys. Rev. C **23**, 1242 (1981).
[23] W. Benenson, D. Mueller, E. Kashy, H. Nann, and L. W. Robinson, Phys. Rev. C **15**, 1187 (1977).
[24] P. Schmalbrock, T. R. Donoghue, M. Wiescher, V. Wijekumar, C. P. Browne, A. A. Rollefson, C. Rolfs, and A. Vlieks, Nucl. Phys. A **457**, 182 (1986).
[25] J. C. Hardy, L. C. Carraz, B. Jonson, and P. G. Hansen, Phys. Lett. B **71**, 307 (1977).
[26] J. C. Hardy and I. S. Towner, Phys. Rev. Lett. **88**, 252501 (2002).
[27] N. B. Gove and M. J. Martin, Atomic Data and Nuclear Data Tables **10**, 205 (1971).
[28] E. Pollacco, L. Trache, E. Simmons, A. Spiridon, M. McCleskey, B. T. Roeder, A. Saastamoinen, R. E. Tribble, G. Pascovici, M. Kebbiri, J. P. Mols, and M. Raillot, Nucl. Instrum. Methods Phys. Res. Sect. A **723**, 102 (2013).